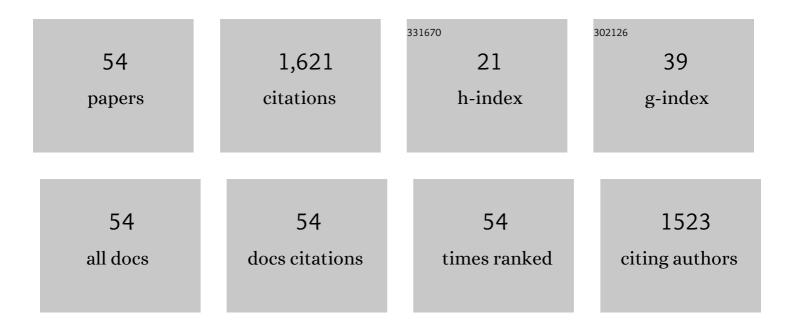
## Lars E Olsson

List of Publications by Year in descending order

Source: https://exaly.com/author-pdf/521864/publications.pdf Version: 2024-02-01



LADS F OLSSON

#	Article	IF	CITATIONS
1	Delayed gadolinium-enhanced MRI of cartilage (dGEMRIC) in early knee osteoarthritis. Magnetic Resonance in Medicine, 2003, 49, 488-492.	3.0	296
2	Gd-DTPA2enhanced MRI of femoral knee cartilage: A dose-response study in healthy volunteers. Magnetic Resonance in Medicine, 2001, 46, 1067-1071.	3.0	119
3	Technical Note: MRI only prostate radiotherapy planning using the statistical decomposition algorithm. Medical Physics, 2015, 42, 6090-6097.	3.0	112
4	Linear energy transfer dependence of a normoxic polymer gel dosimeter investigated using proton beam absorbed dose measurements. Physics in Medicine and Biology, 2004, 49, 3847-3855.	3.0	97
5	MAGIC-type polymer gel for three-dimensional dosimetry: Intensity-modulated radiation therapy verification. Medical Physics, 2003, 30, 1264-1271.	3.0	93
6	MR-OPERA: A Multicenter/Multivendor Validation of Magnetic Resonance Imaging–Only Prostate Treatment Planning Using Synthetic Computed Tomography Images. International Journal of Radiation Oncology Biology Physics, 2017, 99, 692-700.	0.8	82
7	Image artifacts due to a time-varying contrast medium concentration in 3D contrast-enhanced MRA. Journal of Magnetic Resonance Imaging, 1999, 10, 919-928.	3.4	54
8	Measurement of MR signal and T2* in lung to characterize a tight skin mouse model of emphysema using single-point imaging. Journal of Magnetic Resonance Imaging, 2007, 25, 488-494.	3.4	49
9	Magnetic resonance imaging of experimental mouse colitis and association with inflammatory activity. Inflammatory Bowel Diseases, 2006, 12, 478-485.	1.9	48
10	<scp>MR</scp> and <scp>CT</scp> data with multiobserver delineations of organs in the pelvic area—Part of the Gold Atlas project. Medical Physics, 2018, 45, 1295-1300.	3.0	45
11	Ferrous sulphate gel dosimetry and MRI for proton beam dose measurements. Physics in Medicine and Biology, 1999, 44, 1983-1996.	3.0	43
12	Pre-contrast T1 and cartilage thickness as confounding factors in dGEMRIC when evaluating human cartilage adaptation to physical activity. BMC Medical Imaging, 2020, 20, 1.	2.7	41
13	Feasibility assessment of using oxygen-enhanced magnetic resonance imaging for evaluating the effect of pharmacological treatment in COPD. European Journal of Radiology, 2014, 83, 2093-2101.	2.6	30
14	3He MRI-based assessment of posture-dependent regional ventilation gradients in rats. Journal of Applied Physiology, 2005, 98, 2259-2267.	2.5	28
15	Registration free automatic identification of gold fiducial markers in MRI target delineation images for prostate radiotherapy. Medical Physics, 2017, 44, 5563-5574.	3.0	27
16	Clinical validation of a commercially available deep learning software for synthetic CT generation for brain. Radiation Oncology, 2021, 16, 66.	2.7	25
17	Dosimeter Gel and MR Imaging for Verification of Calculated Dose Distributions in Clinical Radiation Therapy. Acta Oncológica, 1997, 36, 283-290.	1.8	24
18	Dosimetric effects of adaptive prostate cancer radiotherapy in an MR-linac workflow. Radiation Oncology, 2020, 15, 168.	2.7	24

LARS E OLSSON

#	Article	IF	CITATIONS
19	MR-PROTECT: Clinical feasibility of a prostate MRI-only radiotherapy treatment workflow and investigation of acceptance criteria. Radiation Oncology, 2020, 15, 77.	2.7	24
20	Improvements in absorbed dose measurements for external radiation therapy using ferrous dosimeter gel and MR imaging (FeMRI). Physics in Medicine and Biology, 1998, 43, 261-276.	3.0	23
21	High-throughput magnetic resonance imaging in murine colonic inflammation. Biochemical and Biophysical Research Communications, 2007, 355, 1102-1107.	2.1	22
22	<sup>1</sup> H and hyperpolarized <sup>3</sup> He MR imaging of mouse with LPSâ€induced inflammation. Journal of Magnetic Resonance Imaging, 2009, 29, 977-981.	3.4	22
23	Intensity-based dual model method for generation of synthetic CT images from standard T2-weighted MR images – Generalized technique for four different MR scanners. Radiotherapy and Oncology, 2017, 125, 411-419.	0.6	22
24	A texture analysis approach to quantify ventilation changes in hyperpolarised <sup>3</sup> He MRI of the rat lung in an asthma model. NMR in Biomedicine, 2012, 25, 131-141.	2.8	20
25	Cone beam CT for QA of synthetic CT in MRI only for prostate patients. Journal of Applied Clinical Medical Physics, 2018, 19, 44-52.	1.9	19
26	Image analysis methods for assessing levels of image plane nonuniformity and stochastic noise in a magnetic resonance image of a homogeneous phantom. Medical Physics, 2000, 27, 1980-1994.	3.0	17
27	COPD Patients Have Short Lung Magnetic ResonanceT1Relaxation Time. COPD: Journal of Chronic Obstructive Pulmonary Disease, 2016, 13, 153-159.	1.6	17
28	Target definition in radiotherapy of prostate cancer using magnetic resonance imaging only workflow. Physics and Imaging in Radiation Oncology, 2019, 9, 89-91.	2.9	15
29	Variable flip angle 3D ultrashort echo time (UTE) T <sub>1</sub> mapping of mouse lung: A repeatability assessment. Journal of Magnetic Resonance Imaging, 2018, 48, 846-852.	3.4	13
30	Imaging Biomarkers and Pathobiological Profiling in a Rat Model of Drug-Induced Interstitial Lung Disease Induced by Bleomycin. Frontiers in Physiology, 2020, 11, 584.	2.8	13
31	Separation of arteries and veins using flow-induced phase effects in contrast-enhanced MRA of the lower extremities. Magnetic Resonance Imaging, 2002, 20, 49-57.	1.8	11
32	Influence of age and sex on the longitudinal relaxation time, T1, of the lung in healthy neverâ€smokers. Journal of Magnetic Resonance Imaging, 2016, 43, 1250-1257.	3.4	10
33	Basic concepts and applications of functional magnetic resonance imaging for radiotherapy of prostate cancer. Physics and Imaging in Radiation Oncology, 2019, 9, 50-57.	2.9	10
34	Volumetric modulated arc therapy dose prediction and deliverable treatment plan generation for prostate cancer patients using a densely connected deep learning model. Physics and Imaging in Radiation Oncology, 2021, 19, 112-119.	2.9	10
35	MRI image plane nonuniformity in evaluation of ferrous sulphate dosimeter gel (FeGel) by means of T1-relaxation time. Magnetic Resonance Imaging, 1999, 17, 1357-1370.	1.8	9
36	Airspace Dimension Assessment (AiDA) by inhaled nanoparticles: benchmarking with hyperpolarised 129Xe diffusion-weighted lung MRI. Scientific Reports, 2021, 11, 4721.	3.3	9

LARS E OLSSON

#	Article	IF	CITATIONS
37	Prospective Clinical Feasibility Study for MRI-Only Brain Radiotherapy. Frontiers in Oncology, 2021, 11, 812643.	2.8	9
38	Airspace Dimension Assessment with nanoparticles reflects lung density as quantified by MRI. International Journal of Nanomedicine, 2018, Volume 13, 2989-2995.	6.7	8
39	Repeatability and reproducibility of longitudinal relaxation rate in 12 small-animal MRI systems. Magnetic Resonance Imaging, 2019, 59, 121-129.	1.8	8
40	T1 Relaxation Time in Lungs of Asymptomatic Smokers. PLoS ONE, 2016, 11, e0149760.	2.5	8
41	Longitudinal Imaging Using PET/CT with Collagen-I PET-Tracer and MRI for Assessment of Fibrotic and Inflammatory Lesions in a Rat Lung Injury Model. Journal of Clinical Medicine, 2020, 9, 3706.	2.4	7
42	Investigation of the clinical inter-observer bias in prostate fiducial marker image registration between CT and MR images. Radiation Oncology, 2021, 16, 150.	2.7	7
43	Development and evaluation of a deep learning based artificial intelligence for automatic identification of gold fiducial markers in an MRI-only prostate radiotherapy workflow. Physics in Medicine and Biology, 2020, 65, 225011.	3.0	7
44	Imaging Biomarkers in Animal Models of Drug-Induced Lung Injury: A Systematic Review. Journal of Clinical Medicine, 2021, 10, 107.	2.4	7
45	Artificial intelligence and the medical physics profession - A Swedish perspective. Physica Medica, 2021, 88, 218-225.	0.7	6
46	Verification of Single Beam Treatment Planning Using a Ferrous Dosimeter Gel and MRI (FeMRI). Acta Oncológica, 1998, 37, 561-566.	1.8	5
47	A MRI and Polarized Gases Compatible Respirator and Gas Administrator for the Study of the Small Animal Lung: Volume Measurement and Control. IEEE Transactions on Biomedical Engineering, 2010, 57, 1745-1749.	4.2	5
48	Knee dGEMRIC at 7ÂT: comparison against 1.5ÂT and evaluation of T1-mapping methods. BMC Musculoskeletal Disorders, 2018, 19, 149.	1.9	5
49	In Vivo Measurements of T2 Relaxation Time of Mouse Lungs during Inspiration and Expiration. PLoS ONE, 2016, 11, e0166879.	2.5	5
50	Using Câ€Arm Xâ€ray images from marker insertion to confirm the gold fiducial marker identification in an <scp>MRI</scp> â€only prostate radiotherapy workflow. Journal of Applied Clinical Medical Physics, 2018, 19, 185-192.	1.9	4
51	The change of longitudinal relaxation rate in oxygen enhanced pulmonary MRI depends on age and BMI but not diffusing capacity of carbon monoxide in healthy never-smokers. PLoS ONE, 2017, 12, e0177670.	2.5	4
52	1H and hyperpolarized 3He magnetic resonance imaging clearly detect the preventative effect of a glucocorticoid on endotoxin-induced pulmonary inflammation in vivo. Innate Immunity, 2011, 17, 204-211.	2.4	1
53	High-Resolution MR Imaging of Muscular Fat Fraction—Comparison of Three T2-Based Methods and Chemical Shift-Encoded Imaging. Tomography, 2017, 3, 153-162.	1.8	1
54	Favorable fatty acid composition in adipose tissue in healthy Iraqi- compared to Swedish-born men — a pilot study using MRI assessment. Adipocyte, 2022, 11, 153-163.	2.8	1